Discrimination of Potent Inhibitors of *Toxoplasma gondii* Enoyl-Acyl Carrier Protein Reductase by a Thermal Shift Assay

Gustavo A. Afanador,[†] Stephen P. Muench,[‡] Martin McPhillie,[§] Alina Fomovska,[‖] Arne Schön,[⊥] Ying Zhou,[‖] Gang Cheng,[@] Jozef Stec,[#] Joel S. Freundlich,[▽] Hong-Ming Shieh,[○] John W. Anderson,[○] David P. Jacobus,[○] David A. Fidock,[●] Alan P. Kozikowski,[@] Colin W. Fishwick,[▲] David W. Rice,[§] Ernesto Freire,[⊥] Rima McLeod,[‖] and Sean T. Prigge*,[†]

[†]Department of Molecular Microbiology and Immunology, Johns Hopkins Bloomberg School of Public Health, Baltimore, Maryland 21205, United States

[‡]School of Biomedical Sciences, University of Leeds, Leeds LS2 9JT, U.K.

[§]Department of Molecular Biology and Biotechnology, University of Sheffield, Sheffield S10 2TN U.K.

[‖]Department of Ophthalmology and Visual Sciences, Pediatrics (Infectious Diseases), Committees on Genetics, Immunology, and Molecular Medicine, Institute of Genomics and Systems Biology, and The College, The University of Chicago, Chicago, Illinois 60612, United States

[⊥]Department of Biology, The Johns Hopkins University, Baltimore, Maryland 21218, United States

[@]Drug Discovery Program, Department of Medicinal Chemistry and Pharmacognosy, University of Illinois at Chicago, Chicago, Illinois 60612, United States

[#]College of Pharmacy, Chicago State University, DH 203-3, 9501 South King Drive, Chicago, Illinois 60628, United States

[▽]Department of Pharmacology and Physiology and Department of Medicine, Center for Emerging and Reemerging Pathogens, Rutgers University-New Jersey Medical School, 185 South Orange Avenue, Newark, New Jersey 07103, United States

[○]Department of Medicinal Chemistry, Jacobus Pharmaceutical Company, Princeton, New Jersey 08540, United States

[●]Department of Microbiology and Immunology and Division of Infectious Diseases, Department of Medicine, Columbia University Medical Center, New York, New York 10032, United States

[▲]School of Chemistry, University of Leeds, Leeds LS2 9JT, U.K.

ABSTRACT: Many microbial pathogens rely on a type II fatty acid synthesis (FASII) pathway that is distinct from the type I pathway found in humans. Enoyl-acyl carrier protein reductase (ENR) is an essential FASII pathway enzyme and the target of a number of antimicrobial drug discovery efforts. The biocide triclosan is established as a potent inhibitor of ENR and has been the starting point for medicinal chemistry studies. We evaluated a series of triclosan analogues for their ability to inhibit the growth of *Toxoplasma gondii*, a pervasive human pathogen, and its ENR enzyme (*Tg*ENR). Several compounds that inhibited *Tg*ENR at low nanomolar concentrations were identified but could not be further differentiated because of the limited dynamic range of the *Tg*ENR activity assay. Thus, we adapted a thermal shift assay (TSA) to directly measure the dissociation constant (K_d) of the most potent inhibitors identified in this study as well as inhibitors from previous studies. Furthermore, the TSA allowed us to determine the mode of action of these compounds in the presence of the reduced nicotinamide adenine dinucleotide (NADH) or nicotinamide adenine dinucleotide (NAD$^+$) cofactor. We found that all of the inhibitors bind to a *Tg*ENR−NAD$^+$ complex but that they differed in their dependence on NAD$^+$ concentration. Ultimately, we were able to identify compounds that bind to the *Tg*ENR−NAD$^+$ complex in the low femtomolar range. This shows how TSA data combined with enzyme inhibition, parasite growth inhibition data, and ADMET predictions allow for better discrimination between potent ENR inhibitors for the future development of medicine.
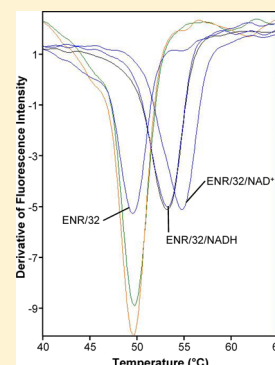
Toxoplasma gondii is an obligate intracellular, protozoan parasite that infects approximately one-third of the world's population, causing substantial morbidity and mortality.[1−6] The life cycle of *T. gondii* is comprised of a sexual phase that takes place only in the primary host (cats of the Felidae family) and an asexual phase that can occur in any warm-blooded animal, including humans.[7,8]

Currently, there is no available vaccine to prevent infection in humans, and only the antifolate medicines sulfadiazine and

pyrimethamine are typically used for treatment of *T. gondii* in humans.[2,9] Sulfonamides are associated with hypersensitivity, and pyrimethamine is associated with bone marrow toxicity. Even though these medications are effective against tachyzoites, the obligate intracellular form of the parasite in the acute stage of the disease, they are ineffective against the encysted, latent bradyzoites. There is no available treatment that eliminates bradyzoites in humans.[10] *T. gondii* infection in immunocompetent individuals is generally asymptomatic and self-limiting, whereas in immunocompromised people, *T. gondii* infection can cause eye and brain disease such as toxoplasmic encephalitis and chorioretinitis and in severe cases can be fatal.[11,12] Pregnant women are especially at risk because the parasite can be transmitted from mother to fetus and can lead to congenital toxoplasmosis that may result in abortion, neonatal death, or fetal abnormalities.[2,9,13−18]

T. gondii parasites contain a plastid organelle, called the apicoplast, which harbors plantlike metabolic pathways.[19] One pathway that resides in the apicoplast is the machinery for a type II fatty acid synthesis (FASII) pathway that is prokaryotic-like.[20,21] The FASII pathway in *T. gondii* has been shown to be essential for parasite survival, making it an attractive target for drug discovery efforts.[22−26] In malaria parasites, a similar FASII pathway is critical for liver stage development[27,28] and is thought to have an important role in the synthesis of lipoic acid.[29] In contrast to the type II pathway, humans rely on a distinct type I pathway for bulk fatty acid synthesis, which is encoded in a single polypeptide chain.[30] Fatty acid biosynthesis is an iterative process involving the condensation of malonyl-CoA with a nascent fatty acid chain that is covalently bound to acyl carrier protein (ACP). The enzyme enoyl-ACP reductase (ENR) is responsible for the final reductive step in each round of fatty acid chain elongation, the NADH-dependent reduction of *trans*-2-enoyl-ACP to acyl-ACP.[31] Many inhibitors of bacterial and parasitic ENR enzymes have been previously described, including diazaborines, isoniazid, and triclosan.[32−34] It has been shown that triclosan inhibits *T. gondii* ENR (*Tg*ENR) with an IC_{50} value of <20 nM in an *in vitro* inhibition assay using pure recombinant *Tg*ENR.[35] Triclosan also inhibits the growth of *T. gondii* parasites with an IC_{50} of ∼200 nM, presumably because of its inhibition of the FASII pathway.[23]

Even though triclosan is a potent inhibitor of *Tg*ENR, it has limitations, including poor bioavailability and impairment of muscle contractility, that prevent it from being a safe and effective medicine.[36] Instead, triclosan has been exploited as a scaffold to generate a series of analogues, many of which are also potent inhibitors of *Tg*ENR.[35,37−39] In this study, we report the inhibitory properties of a set of 2′-, 4′-, 5-, and 6-substituted triclosan analogues developed as inhibitors of *Plasmodium falciparum* ENR (*Pf*ENR) and *Mycobacterium tuberculosis* ENR (*Mt*InhA).[27,40−43] Several of these compounds inhibited *Tg*ENR at low nanomolar concentrations, the lowest concentrations that we are able to assess in our enzymatic activity assay. To further characterize the inhibitory properties of these compounds and potent inhibitors from previous medicinal chemistry efforts,[37,38] we employed a thermal shift assay (TSA). Using this assay, we were able to confirm the mode of action for all of the compounds as binding to the *Tg*ENR−NAD⁺ complex rather than to the *Tg*ENR−NADH complex or to *Tg*ENR alone. Using thermodynamic parameters determined by differential scanning calorimetry, we calculated dissociation constants[44−46] for binding of NAD⁺ and NADH to *Tg*ENR as well as for binding of the inhibitor to the *Tg*ENR−NAD⁺ complex. The K_d values we

determined range from 6 mM (for binding of NAD⁺ to *Tg*ENR) to 6.3 fM (for binding of compound **19** to the *Tg*ENR−NAD⁺ complex), highlighting the large dynamic range of the TSA. Consequently, TSA results combined with enzyme and parasite inhibition data provide a better basis for differentiating between potent ENR inhibitors.

■ MATERIALS AND METHODS

Compound Preparation and Synthesis. Compounds were designed and synthesized as described by A. Kozikowski[37,38] and Jacobus Pharmaceutical Inc.[27,40−43] The purity of compounds **1−4**,[43] **5−10**,[40] **11−14**,[41,42] **15−18**,[27] **19−29**,[38] and **30−32**[37] was >95% as determined by high-performance liquid chromatography, and the identity of each compound was verified by high-resolution mass spectrometry. The compounds were initially dissolved in dimethyl sulfoxide (DMSO) at a concentration of 10 mM and further diluted to required concentrations in culture media (described below). For cell proliferation assays, the final concentration of DMSO was not more than 0.1%, whereas for the *in vitro Tg*ENR enzyme assay, the DMSO concentration was 1%.

Parasite and Cell Culture. The strain of *T. gondii* parasites used in this set of experiments was a modified type I RH strain that expresses yellow fluorescent protein (RH-YFP), kindly provided by B. Striepen (University of Georgia, Athens, GA). Parasites were maintained in confluent monolayers of human foreskin fibroblast (HFF) cells at 37 °C and 5% CO_2 in culture medium consisting of Iscove's Modified Dulbecco's Medium supplemented with 10% fetal calf serum, 1% Glutamax, and 1% penicillin/streptomycin/fungizone (Invitrogen).

***In Vitro* Challenge Assay.** Growth inhibition of *T. gondii* was assessed as previously described.[38] Host cells containing RH-YFP parasites were lysed by being passed twice through a 25 gauge needle and separated from the parasites by filtration and centrifugation. Confluent monolayers of HFF cells in 96-well plates (Falcon 96 Optilux Flat-bottom) were infected with 3500 parasites per well. Parasites were allowed to infect host cells for 1 h, after which experimental compounds and control solutions were added. Seventy-two hours later, the parasite burden was assessed by measuring the relative fluorescence using a Synergy H4 Hybrid Reader (BioTek) and Gen5 version 1.10. All compounds and control solutions were tested in triplicate exemplars. Biological replicates of each experiment were performed twice for compound **17** and three times for all other compounds. The compounds were tested in a dilution series from 10 to 0.01 μM as described previously.[38] In each assay, these results were compared with those for the DMSO control and triclosan. Other internal controls included a curve obtained with varying concentrations of parasites to confirm that each assay detected differing numbers of parasites, and cultures treated with a known inhibitory concentration of pyrimethamine and sulfadiazine as a positive control. The inhibitory index was calculated as $[RFU_{(compound)} − RFU_{(control\ fibroblasts)}]/[RFU_{(DMSO\ control)} − RFU_{(control\ fibroblasts)}] \times 100$. MIC_{50} is defined as the compound concentration required to inhibit replication by 50%.

Human Cell Proliferation Assay. Potential cytotoxic effects of the compounds were assessed using Cell Proliferation Reagent WST-1 (Roche), which measures the metabolic activity of viable cells. Confluent HFF cells in 96-well plates were treated under the same conditions as in the challenge assay described above, except that the cells were not infected with parasites. After 72 h, the cells were incubated with WST-1 reagent for 1−2 h, and cell

viability was assessed by measuring the absorbance at 420 nm of the final colored product, which correlates directly with the cell number. All samples were tested in triplicate in at least two biological replicates.

Inhibition of *Tg*ENR Activity *in Vitro* and Enzymatic Assay. Recombinant *Tg*ENR was purified as described previously.[47] A 96-well plate assay was used to assess the inhibition of *Tg*ENR as described previously.[37,38] Briefly, a SpectraMax M2 plate reader was used to monitor the activity of *Tg*ENR by consumption of NADH (ε_{340} = 6220 M^{-1} cm^{-1}). Reactions were conducted in a final volume of 100 μL in 96-well Corning UV plates. A reaction mixture containing 100 μM crotonyl-CoA (Sigma), 1 μL of DMSO (or compounds dissolved in DMSO), 5 nM *Tg*ENR, 100 mM sodium/potassium phosphate (pH 7.5), 150 mM NaCl, and 100 μM NADH was used. The enzymatic activity was determined by comparing the slopes of the absorbance curves for each well to those of the blanks in the first column of the plate. Each compound was measured in duplicate at a final concentration of 1 μM. Potent inhibitors (>90% inhibition at 1 μM) were further analyzed to determine IC_{50} values in triplicate. Nonlinear regression analysis was performed using GraphPad Prism.

To calculate the K_m and k_{cat} values for NADH and crotonyl-CoA, we followed a method described previously.[25] K_m and k_{cat} were determined at variable concentrations of NADH (0−0.5 mM) in triplicate and a fixed concentration of crotonyl-CoA (100 μM). K_m and k_{cat} for crotonyl-CoA were determined at concentrations ranging from 0.8 to 150 μM and a fixed concentration of NADH (100 μM). Kinetic parameters were calculated by fitting the initial velocity data to the Michaelis−Menten equation using GraphPad Prism.

Thermal Shift Assay (TSA). A real-time polymerase chain reaction (RT-PCR) instrument, in the presence of Sypro Orange (an environmentally sensitive fluorescent dye), was used to monitor the thermal unfolding of *Tg*ENR alone or in the presence of ligands. The TSA was modified from previous reports[44−46] to measure the thermal melting temperature (T_m) of *Tg*ENR. RT-PCR tube strips (Eppendorf) were used to hold 31 μL mixtures containing final concentrations of 2 μM *Tg*ENR, 20 μM inhibitor, and 100 μM cofactor. The reaction mixtures were set up with a 28 μL mixture of *Tg*ENR and buffer [20 mM HEPES (pH 7.5) and 100 mM NaCl] to which 1 μL of water (or cofactor dissolved in water), 1 μL of DMSO (or inhibitor dissolved in DMSO), and 1 μL of Sypro Orange (Sigma, product no. S-5692 at a final concentration of 5×) were added. The reaction mixture was incubated in the RT-PCR machine (Applied Biosystems, Step One Plus Real-Time PCR System) for 2 min at 20 °C followed by 0.2 °C increases in the temperature every 10 s until a final temperature of 80 °C had been reached. During the thermal scan, fluorescence was monitored using a predefined TAMRA filter in which an increase in Sypro Orange fluorescence was observed upon thermal denaturation of *Tg*ENR. The derivative of the fluorescence curve was used to determine the T_m (as seen in Figure 1). The initial T_m in the absence of ligands, but in the presence of DMSO, served as the baseline temperature (T_o) for determining temperature shifts (ΔT_m). All measurements were taken in triplicate.

Calculation of the Binding Constant (K_d). The T_m values obtained in the TSA were used to calculate the dissociation constant (K_d) as described by Mei-Chu Lo and co-workers.[44] The
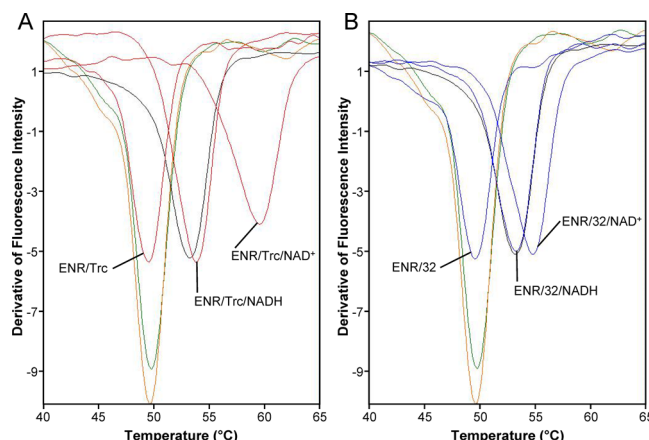
Figure 1. Thermal shift assay results for triclosan (red) and compound **32** (blue). The derivatives of the fluorescence intensity curves are shown with the minima defining the melting temperatures (T_m): green for enzyme alone, black for enzyme with NADH, and orange for enzyme with NAD$^+$.

dissociation constant at the melting temperature was calculated using the equation

$$K_{d(T_m)} = [L_{T_m}]/\left(\exp\left\{\frac{-\Delta H_{T_o}}{R}\left(\frac{1}{T_m} - \frac{1}{T_o}\right)\right.\right.$$
$$\left.\left. + \frac{\Delta C_{pT_o}}{R}\left[\ln\left(\frac{T_m}{T_o}\right) + \frac{T_o}{T_m} - 1\right]\right\}\right)$$

where T_o is the melting temperature of *Tg*ENR with no ligands (baseline), T_m is the melting temperature of *Tg*ENR in complex with one or more ligands, R is the gas constant, ΔH is the enthalpy of protein unfolding, ΔC_p is the heat capacity change on protein unfolding, and $[L_{T_m}]$ is the free ligand concentration at T_m. The two thermodynamic parameters (ΔH and ΔC_p) were measured by differential scanning calorimetry (DSC). A temperature scan of 0.33 mg/mL *Tg*ENR from 10 to 65 °C at a rate of 1 °C/min was monitored using a VP-DSC microcalorimeter (MicroCal). The change in heat capacity (ΔC_{pT_o}) of 3.8 kcal K^{-1} mol^{-1} was estimated from the difference in baselines between the baselines of the denatured and native states. The enthalpy (ΔH_{T_o}) was obtained from the area under the curve yielding a value of 228.7 kcal/mol. The dissociation constant at the melting temperature was normalized to temperature T (37 °C) using the equation

$$K_{d(T)} = \frac{K_{d(T_m)}}{\exp\left[\frac{-\Delta H_{L(T)}}{R}\left(\frac{1}{T} - \frac{1}{T_m}\right)\right]}$$

where $\Delta H_{L(T)}$ is the van't Hoff enthalpy of binding at temperature T, estimated to be −15 kcal/mol.[44,48]

Molecular Docking. Molecular docking studies were performed using AutoDock version 4.2,[49] SwissPDB Viewer,[50] and MacroModel version 8.1 (Schrodinger, LLC, New York, NY) in conjunction with the X-ray crystal structures of *Tg*ENR in complex with inhibitors triclosan [Protein Data Bank (PDB) entry 2O2S][51] and benzimidazole (PDB entry 1LX6).[52] A 10 Å radius of the active site was used to dock the synthesized molecules with a grid box margin of 62. All other docking parameters were left as

default values. The obtained docking poses were analyzed using PyMol.

■ RESULTS AND DISCUSSION

Parasite Inhibition, Host Cell Cytotoxicity, and Inhibition of TgENR Enzymatic Activity. A structure-based approach was adopted by Freundlich and colleagues to develop 2′-, 4′-, 5-, and 6-substituted triclosan analogues against PfENR and MtInhA.[27,40−43] In this study, we evaluated 18 of these analogues against *T. gondii*. The triclosan analogues were first tested for efficacy against *T. gondii* tachyzoites *in vitro*. Triclosan was also included in the assay for a direct comparison. Type 1 RH tachyzoites that express yellow fluorescent protein (RH-YFP) were used, allowing parasite proliferation to be assessed by means of a fluorometric assay, because relative fluorescence is directly correlated with parasite viability. A 72 h end point was chosen to allow slow-acting compounds to take effect. Seven compounds emerged as the most effective inhibitors of *T. gondii* tachyzoites: **5**, **8**−**10**, and **15**−**17** (Table 1). These compounds demonstrated an efficacy equivalent to that of triclosan (MIC$_{50}$ of 2.8 μM), with MIC$_{50}$ values ranging from 1.6 to 3.5 μM. The compounds were also tested for cytotoxic activity against human foreskin fibroblast host cells and exhibited no cytotoxic effects at the highest concentration tested (10 μM). These results demonstrate that inhibition of parasite growth at lower concentrations did not result from killing the host cells; however, because we did not reach the MIC$_{50}$ for inhibition of host cell proliferation, we do not know the overall selectivity of our compounds.

The triclosan analogues were also screened in duplicate at 1 μM for inhibition of TgENR in an *in vitro* inhibition assay. Those analogues with significant inhibitory activity (>90% at 1 μM) were subsequently assayed in triplicate to determine their IC$_{50}$ values (Table 1). A total of six analogues were potent inhibitors of TgENR with IC$_{50}$ values of <23 nM, similar to that of triclosan (15 nM). None of the compounds with 2′-substitutions proved to have significant inhibitory activity. This result is consistent with a lack of potent activity against PfENR.[43] On the basis of the current crystal structures of TgENR and PfENR bound to triclosan,[51] the 2′-triclosan analogues are unlikely to be effective because added bulk at this position will likely result in severe steric clashes with the NAD$^+$ cofactor (see docking results for further details). Potent inhibitors of TgENR with IC$_{50}$ values in the low nanomolar range were found with substitutions at the 4′-, 5-, and 6-positions of triclosan. Previous medicinal chemistry efforts targeting TgENR led to the discovery of several potent 4′-triclosan and 5-triclosan analogues.[37,38] The activities of 6-triclosan analogues have not previously been described against *T. gondii*. However, as shown in Table 1, 6-triclosan analogues such as **15** and **17** can be inhibitors of TgENR enzymatic activity and parasite growth.

Thermal Shift Assay (TSA). Our current study of 18 triclosan analogues yielded six compounds with TgENR IC$_{50}$ values in the low nanomolar range (<23 nM). These IC$_{50}$ values are similar to that of triclosan (15 nM) and approach the low nanomolar concentrations of TgENR used in our activity assay. Because of this, we could not determine which of the six compounds is the most potent or how they compare to triclosan with currently available assays. In addition, we tested 14 inhibitors discovered in previous studies[37,38] that also inhibit TgENR with IC$_{50}$ values of <100 nM, making 20 compounds in total. In an attempt to differentiate among these inhibitors, we adapted a TSA[44−46] to further characterize the binding of the compounds to TgENR.
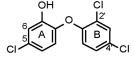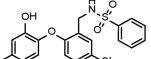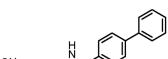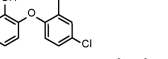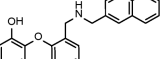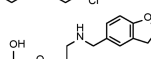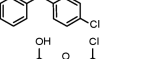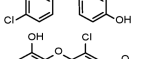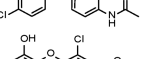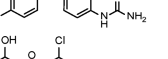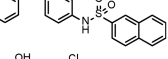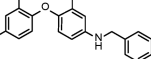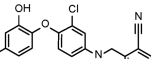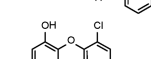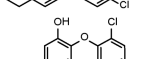
A significant advantage of TSA over several other biophysical techniques, such as nuclear magnetic resonance, mass spectrometry, or calorimetry, is that it can be done with higher throughput without requiring large amounts of protein.[44−46,48,53−55] This method has been previously employed for screening conditions that stabilize proteins;[46,56,57] for K_d calculations for proteins with one or two ligands;[44,45,48,55] and to determine the mode of action of ligand binding.[55] Calculations of K_d values by the TSA have been favorably compared to measurements via other biophysical techniques.[44]
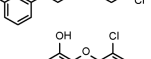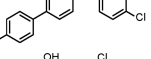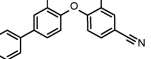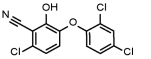
We used the TSA to measure the melting temperature (T_m) of TgENR alone, in a binary complex with a NADH or NAD$^+$ cofactor, or in a ternary complex with triclosan (or analogues) and NADH or NAD$^+$ bound. Using a RT-PCR machine to accurately control the temperature, we monitored the thermal denaturation of TgENR in the presence of the environmentally sensitive dye Sypro Orange. The TSA method consists of monitoring the fluorescence of the dye that has a higher quantum yield when it interacts with hydrophobic amino acids exposed upon TgENR unfolding. As shown in Figure 1, the derivative of the fluorescence intensity is marked by a sharp minimum at the T_m. A shift in thermal stability occurs upon formation of a ligand complex, and the magnitude of the shift in T_m depends on the affinity of the ligand for TgENR. The observed change in T_m [$\Delta T_m = T_m$ (ligand) $- T_o$ (no ligand)] is used to calculate the binding constant (K_d) of the ligand.[44,46] TSA can be particularly useful for proteins such as TgENR that have multiple ligand binding sites and can bind inhibitors and cofactor molecules. In cases like this, the relative stability of the protein with different combinations of ligands can be used to determine the mode of action of an inhibitor.[55]

Binary Complex of TgENR with NADH or NAD$^+$. We studied the ΔT_m of TgENR with increasing concentrations of NADH or NAD$^+$ (Figure 2A). Each data point with a non-zero ΔT_m allowed us to calculate independent K_d values for these ligands. For NADH, K_d values of 26 μM ($\Delta T_m = 0.4$ °C) and 21 μM ($\Delta T_m = 1.7$ °C) were measured, and for NAD$^+$, the K_d values were 6 mM ($\Delta T_m = 0.4$ °C) and 6 mM ($\Delta T_m = 1.6$ °C). The K_d values resulting from the larger temperature shifts are likely to be the most accurate (21 μM for NADH and 6 mM for NAD$^+$). The K_d for binding of NADH to TgENR is similar to the value obtained for PfENR with a K_d for NADH of 51.6 μM[58] and that of *Escherichia coli* ENR (*Ec*ENR) with a K_d for NADH of 5.4 μM.[32] The K_d for NAD$^+$ could not be determined for PfENR, except in the presence of triclosan, yielding an artificially low value of 15 μM,[58] whereas the K_d of NAD$^+$ for *Ec*ENR was determined to be 1.8 mM.[32] The kinetic parameters for TgENR were calculated by using the enzymatic activity assay at 11 different concentrations of NADH and crotonyl-CoA in triplicate, the highest concentration being 500 μM, and dilutions by factors of 2 for NADH and 0.8−150 μM for crotonyl-CoA. Figure 2B shows a Michaelis−Menten plot for TgENR with a k_{cat} of 12 s^{-1} and a K_m of 20 μM for NADH; for crotonyl-CoA, k_{cat} is 26 s^{-1} and K_m is 40 μM (Figure 2C). These values are similar to those of ENR enzymes from the apicomplexan parasites *Eimeria tenella* and *P. falciparum* (Table 2).[25,59,60] Although K_m values cannot be equated with dissociation constants, the K_m values for NADH are consistent with the K_d value of 21 μM determined by the TSA.

Inhibitor Mode of Action Determined by the TSA. The mode of action of ENR inhibition by triclosan has been well studied in several systems, including apicomplexan parasites, plants, and bacteria. Triclosan is an uncompetitive inhibitor with respect to NAD$^+$ and forms a tight ternary triclosan−NAD$^+$−ENR

Table 1. Inhibitory Activities, Toxicities, and Calculated Physicochemical Properties of 18 Substituted Triclosan Inhibitors of *Pf*ENR and *Mt*InhA

Compd.	Structure	Cell Growth Inhibition		*Tg*ENR Inhibition			Physicochemical Properties (ACD/Labs) [e]		
		T. gondii MIC$_{50}$ (μM) [a]	HFF MIC$_{50}$ (μM) [b]	Inhibition at 1 μM (%) [c]	IC$_{50}$ (nM)	95% Conf. Interval (nM)	clogP [d]	TPSA [Å^2]	Sw (mg/L)
Triclosan		2.8 ± 0.2	>10	98 ± 2	15	7-33	5.53	53.25	4.6 [f]
1		>10	>10	13 ± 13	nd		5.59	84.01	2.2
2		>10	>10	14 ± 7	nd		7.46	41.49	0.52
3		>10	>10	22 ± 2	nd		6.74	41.49	0.33
4		>10	>10	28 ± 5	nd		5.63	50.72	4.2
5		3.1 ± 0.3	>10	97 ± 2	3	2-5	4.44	49.69	140
6		10	>10	73 ± 5	nd		4.09	58.56	12
7		>10	>10	74 ± 3	nd		3.82	84.58	7.4
8		3.0 ± 0.8	>10	45 ± 4	nd		6.62	84.01	0.077
9		3.5 ± 0.4	>10	98 ± 2	13	10-16	6.06	41.19	1.0
10		1.6 ± 0.3	>10	96 ± 0	16	13-20	5.64	65.28	2.1
11		>10	>10	97 ± 1	8	7-9	5.55	29.46	2.5
12		>10	>10	78 ± 1	nd		5.82	49.69	2.8
13		>10	>10	80 ± 2	nd		5.53	49.69	4.6
14		>10	>10	41 ± 1	nd		3.82	66.14	6.9
15		2.9 ± 0.4	>10	95 ± 1	18	16-20	5.33	53.25	7.3
16		2.7 ± 0.6	>10	87 ± 2	nd		5.67	29.46	1.9
17		2.8 ± 0.7	>10	92 ± 0	23	19-26	4.44	49.69	21
18		>10	>10	81 ± 1	nd		8.26	29.46	0.024

[a]MIC$_{50}$ of *T. gondii* growth with the SEM from assays conducted in at least two independent trials each with triplicate measurements. [b]Growth inhibition of human foreskin fibroblasts (HFF). [c]Standard deviation from duplicate measurements. [d]Calculated with ChemDraw Ultra version 7.0. [e]These data were predicted by ADMET suite 5.0 (ACD/Laboratories). TPSA is the topological polar surface area and Sw the solubility in water. [f]The actual water solubility for triclosan is 12 mg/L at 20 °C, according to the U.S. Environmental Protection Agency's Rreregistration Eligibility Decision (RED) for triclosan.
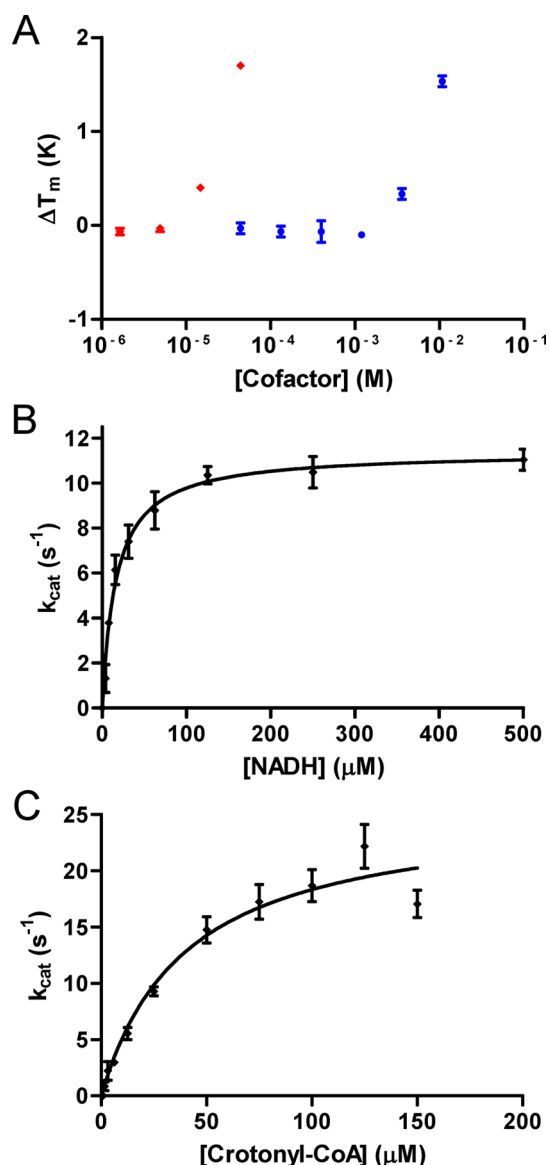
Figure 2. (A) Thermal shift assay results for the binding of NADH (red) and NAD$^+$ (blue) to TgENR. (B) Kinetic analysis of TgENR with the NADH cofactor. (C) Kinetic analysis of TgENR with the crotonyl-CoA cofactor. Error bars represent the standard deviation from triplicate measurements.

Table 2. Kinetic Parameters of Apicomplexan ENR Enzymes

organism	K_m (μM)	standard error (μM)[b]	k_{cat} (s^{-1})	standard error (s^{-1})[b]	ref
		NADH			
E. tenella	60		11		25
P. falciparum	30		49		59
T. gondii[a]	20	3.5	12	0.5	this study[a]
		Crotonyl-CoA			
E. tenella	40		6		25
P. falciparum	48		10		59
T. gondii[a]	40	6.7	26	1.6	this study[a]
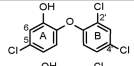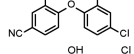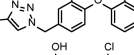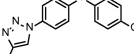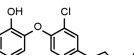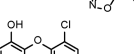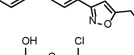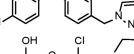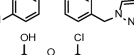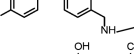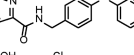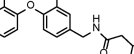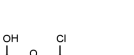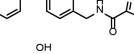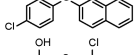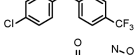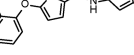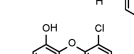
[a]Kinetic measurements were taken in triplicate, and the data were analyzed with GraphPad Prism. [b]Standard error as reported in GraphPad Prism.

complex. Consistent with this mechanism of action, we observed a large shift in T_m when TgENR was analyzed by the TSA in the presence of triclosan and NAD$^+$, but not in the absence of the cofactor (Figure 1A). Interestingly, we also observed a small shift in T_m when triclosan was added to TgENR in the presence of NADH (Figure 1A). Triclosan has an apparent K_d value of 186 μM for the TgENR−NADH complex, an affinity that is probably too weak to have physiological significance because this value is 100000 times larger than the K_d of binding of triclosan to the TgENR−NAD$^+$ complex [1.3 nM at 100 μM NAD$^+$ (Table 3)]. The apparent weak binding of triclosan to the TgENR−NADH complex is consistent with reports of ternary triclosan−NADH complexes formed by ENR enzymes from *E. coli*,[61] *Haemophilus influenza*,[62] and *Pseudomonas aeruginosa*.[63]

Potent inhibition of ENR enzymes with triclosan is caused by the slow formation of a tight ternary triclosan−NAD$^+$−ENR complex. PfENR is 50% identical to TgENR and serves as a good

example of this phenomenon. Triclosan binds to the PfENR−NAD$^+$ complex with a relatively low affinity (53 nM) followed by the slow (forward rate constant of 0.055 s^{-1}) formation of a tight binding complex with an overall inhibition constant of 96 pM.[64] The tight binding complex involves the formation of an α-helix over the inhibitor binding site, a feature that was observed in the crystal structure of TgENR cocrystallized with triclosan and NAD$^+$, making it very likely that triclosan inhibits TgENR through the same mechanism described for other ENR enzymes.[51] The slow kinetics of inhibition appear to be responsible for the artificially high (15 nM) IC$_{50}$ value of triclosan given in Table 1. The IC$_{50}$ value approaches the theoretical limit (half of the TgENR concentration of 5 nM) when the enzyme is preincubated with triclosan and NAD$^+$, allowing the inhibitory complex to form prior to initiation of the assay. In the TSA experiments, there is a total incubation time of ∼30 min from the time the experiment is set up to the time it reaches T_m. This allows enough time for triclosan to form the tight ternary complex. To confirm this, we set up TSA experiments as explained in Materials and Methods but allowed preincubation for 2 h. This preincubation time did not affect the K_d of triclosan for the enzyme (data not shown). To determine the reproducibility of the TSA measurements, we measured the T_m in four experiments in triplicate on different days for TgENR alone, TgENR in a binary complex with NADH or NAD$^+$, and TgENR in a ternary complex with NAD$^+$ and triclosan. The standard deviations of these measurements were 0.40, 0.56, 0.36, and 0.37 °C, respectively.

All of our potent inhibitors were also tested by the TSA for binding to the TgENR−NAD$^+$ complex, the TgENR−NADH complex, or TgENR alone. In all cases, the inhibitors displayed a mode of action similar to that of triclosan, forming a tight complex with TgENR and NAD$^+$. Figure 1B shows the TSA results for **32**, a compound with a structure that differs significantly from the structure of triclosan, but displays a similar T_m shift profile and thus the same mode of action as triclosan, binding exclusively to the TgENR−NAD$^+$ complex. As shown in Figure 1, the presence of 100 μM NAD$^+$ alone (orange curves) or 20 μM inhibitor alone (green curves) does not shift the T_m of TgENR, and thu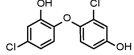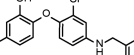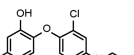s, the ΔT_m observed in the presence of the inhibitor and NAD$^+$ is due to the formation of the ternary complex.

Effect of NAD$^+$ Concentration on Inhibitor Affinity. In TSA experiments, we can control the concentration of cofactors NADH and NAD$^+$. By contrast, in the enzymatic assay, NADH is constantly being consumed and NAD$^+$ is formed over the course of the reaction. For the TSA, we used 100 μM NADH, the concentration used as the starting point in the enzymatic assay. As described above, this concentration is well above the K_d of

Table 3. Thermal Shift Assay Results for Potent Inhibitors of *Tg*ENR from Table 1 and Those Described Elsewhere[37,38]

Compd.	Structure	$TgENR$ Inhibition IC$_{50}$ (nM)	95% Conf. Interval (nM)	K_d (nM) at 100 μM [a]		K_d (fM) at 6 mM [b]		NAD$^+$ K_d Ratio [c]
Triclosan		15	13–22	1.3	± 0.7	20	± 3	62,000
19		24	16–36	1.6	± 0.8	6.3	± 1	250,000
20 [d]		38	30–48	nd		nd		nd
21 [d]		54	43–68	nd		nd		nd
22 [d]		28	22–36	nd		nd		nd
23 [d]		18	14–24	nd		nd		nd
24		26	23–41	680	± 200	2,000	± 300	350,000
25		43	35–54	600	± 30	257	± 40	2,300,000
26		31	26–37	560	± 50	1,800	± 400	310,000
27		19	17–21	6.9	± 2	33	± 5	210,000
28		33	27–40	460	± 5	826	± 90	550,000
29		100	79–126	19,000	± 9,000	116,000	± 50	170,000
30		41	31–54	9,700	± 1,000	887,000	± 100,000	11,000
31		30	25–34	480	± 60	5,300	± 2,000	90,000
32		58	42–79	440	± 30	689	± 40	630,000
5		3	2–5	2.1	± 2	20	± 1	110,000
9		13	10–16	0.8	± 0.2	27.5	± 6	30,000
10		16	13–20	7.3	± 0.2	68.9	± 70	110,000
11		8	7–9	170	± 100	1,000	± 3,000	170,000
15		18	16–20	9.9	± 1	27.5	± 6	360,000
17		23	19–26	210	± 60	939	± 200	220,000

[a]K_d of the inhibitor at a NAD$^+$ concentration of 100 μM with the standard deviation from triplicate measurements. [b]K_d of the inhibitor at a NAD$^+$ concentration of 6 mM with the standard deviation from triplicate measurements. [c]Ratio of the K_d at 100 μM NAD$^+$ to the K_d at 6 mM NAD$^+$. [d]These compounds interfered with the TSA.

NADH (21 μM), ensuring that the majority of *Tg*ENR forms a binary *Tg*ENR−NADH complex during the TSA experiments.

The same is not true for NAD$^+$. In the TSA experiments described above, 100 μM NAD$^+$ was used whereas the K_d is 6 mM.

Under these conditions, the fraction of enzyme found as a binary TgENR–NAD$^+$ complex is very small ($\sim$1.6%).

We then analyzed the binding of two inhibitors, triclosan and **32**, to improve our understanding of how NAD$^+$ concentration affects the apparent K_d values determined by the TSA. We determined K_d values for both inhibitors at eight concentrations of NAD$^+$ ranging from 2.7 μM to 6 mM. As shown in Figure 3A,
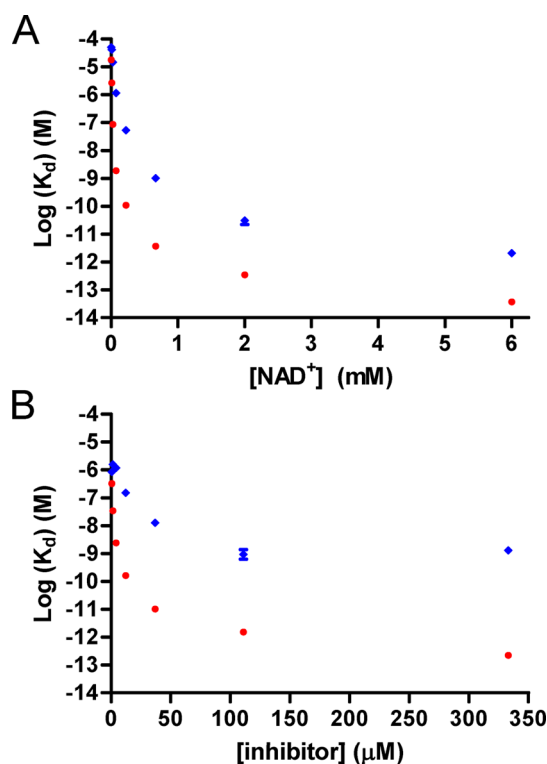

Figure 3. Effect of NAD$^+$ and inhibitor concentration on the apparent dissociation constants of two TgENR inhibitors. The thermal shift assay was used to determine apparent K_d values for triclosan (red) and compound **32** (blue) at different concentrations of NAD$^+$ and inhibitor. (A) The apparent dissociation constants reach a plateau as NAD$^+$ concentrations approach 6 mM (the K_d of NAD$^+$). (B) The apparent dissociation constants decrease as the inhibitor concentration increases to 333 μM, the highest concentration we were able to measure. Error bars represent the standard deviation of triplicate measurements.

the apparent K_d for these inhibitors decreases as the concentration of NAD$^+$ increases, until reaching a plateau while approaching the K_d of NAD$^+$ (6 mM). The apparent dissociation constant of triclosan ranges from 18 μM (at a NAD$^+$ concentration of 2.7 μM) to 20 fM (at a NAD$^+$ concentration of 6 mM), despite the fact that NAD$^+$ is in stoichiometric excess over TgENR (2 μM) throughout this concentration range. Similarly, the K_d values for compound **32** vary from 51 μM to 689 fM over the same range of NAD$^+$ concentrations. These results underscore the need to consider cofactor concentration upon comparison of K_d values for uncompetitive inhibitors like triclosan. For example, a K_d value of 32 nM was reported for binding of triclosan to PfENR,[58] which is similar to the value of 1.3 nM listed in Table 3 for TgENR. However, the K_d for PfENR was determined with 250 μM NAD$^+$, and the equivalent K_d value for TgENR is 105 pM. In a similar experiment, we determined the K_d values for triclosan and compound **32** at seven concentrations ranging from 450 nM to 333 μM while keeping the NAD$^+$ concentration constant at 100 μM. As expected, we found that

the K_d values for both compounds decrease as we increase the inhibitor concentration (Figure 3B).

We determined the K_d values for our most potent TgENR inhibitors in the presence of 6 mM NAD$^+$ and compared these values with those determined at 100 μM NAD$^+$ (Table 3). The higher NAD$^+$ concentration increased the apparent affinity of all of our inhibitors; however, the factor by which the affinity increased was not uniform across the compound series (Table 3). The K_d of **25** decreased by a factor of 2300000 when NAD$^+$ concentrations were increased, whereas the K_d of **30** only decreased by a factor of 11000. Even between similar compounds such as **28** and **29**, there were differences in the dependence of K_d on NAD$^+$ concentration. These differences may reflect the ability of some inhibitors to bind more tightly to TgENR in the absence of NAD$^+$. In the thermodynamic cycle shown in Figure 4A, these
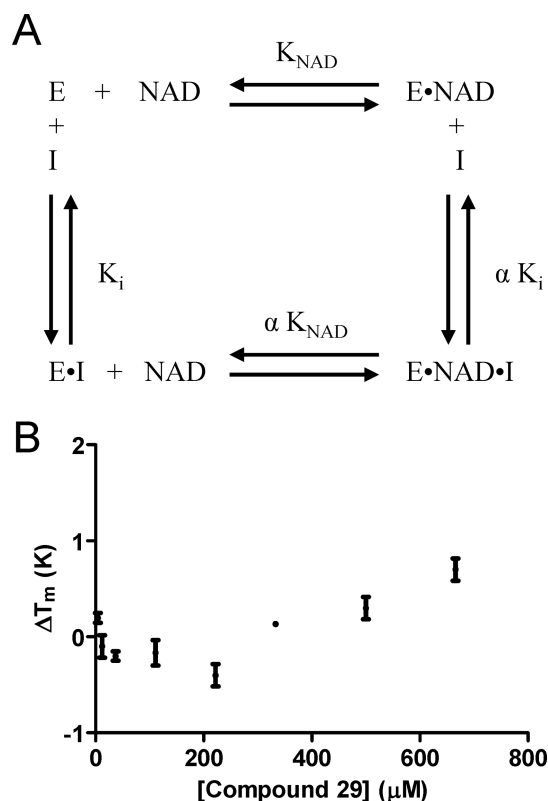
Figure 4. Thermodynamic cycle for the formation of the ternary inhibitor–TgENR–NAD$^+$ complex. The parameter α describes the selectivity of inhibitor binding for the TgENR–NAD$^+$ complex (E·NAD) and the selectivity of binding of NAD$^+$ to the inhibitor–TgENR complex (E·I).

inhibitors would have smaller K_i values and larger α values, indicating less selectivity between binding to the TgENR–NAD$^+$ complex and binding to TgENR alone.

We did not detect the binding of any inhibitor to TgENR when we used an inhibitor concentration of 20 μM; however, K_i values could be well above this level. We screened for inhibitor binding at higher inhibitor concentrations (111 and 333 μM) but found that most compounds did not have measurable binding or interfered with the TSA at these concentrations. Compound **29**, however, appeared to bind with a dissociation constant (K_i) of 0.8 mM (Figure 4B). This value of K_i allows us to estimate the parameter α if we can measure the affinity of compound **29** for the E·NAD complex (αK_i) shown in Figure 4A. The K_d of

compound **29** in the presence of 6 mM NAD$^+$ is 116 pM (Table 3). We can estimate αK_i using the equation for the binding of uncompetitive inhibitors

$$K_i^{app} = \alpha K_i \left(1 + \frac{K_{NAD}}{[NAD]}\right)$$

in which K_i^{app} is the observed dissociation constant of the inhibitor at any concentration of NAD$^+$ and K_{NAD} is the K_d of NAD$^+$. Because the concentration of NAD$^+$ (6 mM) used in the TSA equals K_{NAD}, this equation reduces to

$$\alpha K_i = \frac{K_i^{app}}{2} = 58 \, pM$$

Similar estimations of αK_i can be made for all of the compounds with measured K_d values at 6 mM NAD$^+$ (Table 3). The parameter α describing the selectivity of compound **29** for the binary complex would then be 7×10^{-8}. The parameter α is presumably related to the ratio of K_d values listed in Table 3 in the sense that both numbers provide an indication of how dependent an inhibitor is on binding to the binary TgENR–NAD$^+$ complex. This phenomenon may help to guide the selection of the best inhibitors. The NAD$^+$ concentration has been measured in different cell types, including mouse erythrocytes and mammalian cells, with values of 368 μM and a range of 300–800 μM, respectively.[65−69] Although the concentration of NAD$^+$ in the apicoplast of *T. gondii* has not been measured, it is also likely to be well below the K_d value of 6 mM. Therefore, at any given time, most TgENR molecules will not have NAD$^+$ bound. Indeed, the large discrepancy between the MIC$_{50}$ values in Table 1 and the extremely tight binding properties of some of the compounds in Table 3 may be an indication that NAD$^+$ levels are low in the apicoplast organelle.

Affinities of Inhibitors for the *Tg*ENR–NAD$^+$ Complex. The 20 compounds that we examined by the TSA all had IC$_{50}$ values of <100 nM in the TgENR enzyme activity assay (Table 3). The calculated K_d values at the two NAD$^+$ concentrations can be used to identify the most potent compounds and how dependent inhibitor binding is on NAD$^+$ concentration (Table 3). A total of six compounds exhibited K_d values of <10 nM with 100 μM NAD$^+$ and <100 fM with 6 mM NAD$^+$ (**5**, **9**, **10**, **15**, **19**, and **27**). From an analysis of these compounds, it is clear that tight binding inhibitors can contain small substituents at the 4′-position (as in compound **5**), the 5-position (as in compound **19**), or the 6-position (as in compound **15**). As described previously,[37,38] bulky substituents at the 4′- and 5-positions are accommodated by the TgENR active site. Compound **27** contains a large isoxazole ring at the 5-position, while compounds **9** and **10** contain a benzylamino moiety. The 6-position triclosan analogues have not been described previously for TgENR. We show that modifications at this position are well tolerated as seen for compounds **15** and **17** (see modeling data below).

Overall, three compounds (**5**, **9**, and **19**) appear to bind to the TgENR–NAD$^+$ complex as well as triclosan or better. These compounds differ, however, in terms of how dependent the dissociation constants are on NAD$^+$ concentration. The ratio of K_d values determined at low and high NAD$^+$ concentrations is 250000 for compound **19**, whereas this ratio is only 30000 for compound **9** (Table 3). As discussed above, the weakened dependence of compound **9** on NAD$^+$ concentration could reflect the ability of this compound to bind weakly to TgENR, adding an additional route to forming the ternary inhibitor–TgENR–NAD$^+$ complex.

By contrast, compound **19** may be more dependent on binding to a preformed TgENR–NAD$^+$ complex. In this sense, compound **9** could prove to be a more exciting scaffold for further modification. Because a variety of substituents are tolerated at the 5-position, these are possible additions that could improve the properties of compound **9**. Similarly, small groups such as those found in compounds **15** and **17** could be added to the 6-position.

Inhibitor Modeling. To improve our understanding of the different binding properties of the various inhibitors studied, molecular modeling was conducted using the TgENR crystal structure and the molecular docking software AutoDock.[49] The least effective triclosan analogues contained modifications on the B-ring at the 2′-position. The proximity of the NAD$^+$ cofactor to this position on the B-ring is likely to cause a significant steric clash upon inhibitor binding (Figure 5A). The addition of a
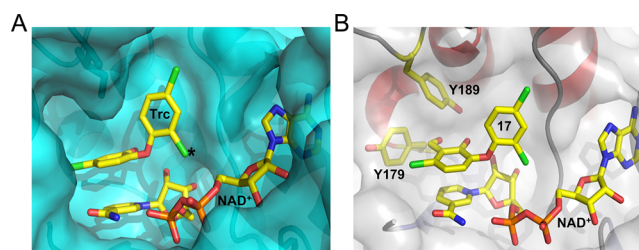
Figure 5. (A) NAD$^+$–triclosan binding pocket of TgENR from a crystal structure (PDB entry 2O2S)[51] Ligands NAD$^+$ and triclosan are shown as sticks colored by atom type. Modification of the atom at the 2′-position (marked with an asterisk) results in decreased affinity (see compounds **1**−**4**) because of steric clashes with the NAD$^+$ cofactor and the binding pocket. (B) Molecular modeling of inhibitor **17** showing the position of the additional OH group and its proximity to the two fully conserved active site Tyr residues.

5-methyl-3-carboxamide-isoxazole group to the A- or B-ring of triclosan resulted in a marked difference in the K_d value. The presence of this group at the 5-position on the A-ring (compound **27**) produced a very potent inhibitor (K_d = 33 fM with 6 mM NAD$^+$), whereas this modification at the 4′-position on the B-ring gave inhibitor **29** with 3500-fold less affinity (K_d = 116 pM with 6 mM NAD$^+$).

Molecular modeling was used to rationalize this difference in affinity. Modeling in AutoDock suggested that the isoxazole group and other large substituents[37,38] can be tolerated within the hydrophobic pocket surrounding the A-ring because of the mobile α-helix. Conversely, the positioning of this group on the B-ring extends toward the solvent-exposed entrance to the binding site and should be able to accommodate such a substituent. However, sampling the potential ligand conformations in AutoDock exposed a steric clash between the 4′-methylisoxazole of compound **29** and Phe243 (TgENR numbering) because of the rigid nature of the 5-methyl-3-carboxamide-isoxazole group. The addition of a methylene group between the amide and isoxazole ring (compound **28**) decreased the K_d by ~2 orders of magnitude, perhaps because the additional flexibility alleviated this steric clash.

The most promising inhibitors discovered to date have a modification at the 6-position on the A-ring. Considering the extra bulk of the nitrile (compound **15**) and the hydroxymethyl (compound **17**) moieties, the initial steric clash observed between these substituents and Tyr179 must be alleviated through the movement about Cβ. This result is corroborated through further modeling studies in which the conserved Tyr179 residue can

rotate to accommodate the substitutents at the 6-position within the heart of the binding site (Figure 5B).

CONCLUSIONS

We evaluated a series of triclosan analogues as inhibitors of *T. gondii*. The 4′- and 5-substituted triclosan analogues are effective inhibitors of parasite growth and *Tg*ENR enzymatic activity. Compounds with modifications at the 2′-position did not show inhibitory activity against *Tg*ENR because of steric clashes with either the NAD$^+$ cofactor or the top of the binding pocket. Modifications at the 6-position were well tolerated and displayed good inhibitory activity against the parasite and the *Tg*ENR enzyme. Six compounds that inhibited *Tg*ENR with IC$_{50}$ values in the low nanomolar range were identified but could not be further differentiated because of the limited dynamic range of the *Tg*ENR activity assay. A thermal shift assay was employed to further characterize these compounds as well as 14 other potent inhibitors from previous studies.[37,38] All 20 compounds share the same mode of action and form a ternary complex with *Tg*ENR and NAD$^+$ but do not bind significantly to the *Tg*ENR−NADH complex or to *Tg*ENR alone. The apparent K_d values for the inhibitors were strongly affected by NAD$^+$ concentration and reached a plateau as the NAD$^+$ concentration approached the K_d of NAD$^+$ (6 mM). By comparing the apparent K_d values of the inhibitors at low and high NAD$^+$ concentrations, we could identify potent compounds that are less dependent on NAD$^+$ binding. Ultimately, we were able to identify six compounds that bind to the *Tg*ENR−NAD$^+$ complex in the low femtomolar range with affinities similar to or exceeding that of triclosan (**5, 9, 10, 15, 19**, and **27**). Additionally, four of these compounds inhibit the growth of *T. gondii* parasites with potency equal to or better than that of triclosan (**5, 9, 10**, and **15**). TSA data combined with enzyme inhibition and parasite growth inhibition data allow for better discrimination between potent ENR inhibitors and therefore provide an excellent method for better selection of promising lead compounds.

AUTHOR INFORMATION

Corresponding Author
*E-mail: sprigge@jhsph.edu. Phone: (443) 287-4822

Notes
The authors declare no competing financial interest.

ABBREVIATIONS

acetyl-CoA, acetyl-coenzyme A; ACP, acyl carrier protein; CoA, coenzyme A; ENR, enoyl-ACP reductase; FASII, type II fatty acid synthesis pathway; HFF, human foreskin fibroblasts; NADH, reduced nicotinamide adenine dinucleotide; SEM, standard error of the mean; *Tg*ENR, *T. gondii* enoyl-ACP reductase; TPSA, topological polar surface area; S_w, solubility in water.

REFERENCES

(1) Hill, D., and Dubey, J. P. (2002) *Toxoplasma gondii*: Transmission, diagnosis and prevention. *Clin. Microbiol. Infect.* 8, 634−640.

(2) McLeod, R., Boyer, K., Karrison, T., Kasza, K., Swisher, C., Roizen, N., Jalbrzikowski, J., Remington, J., Heydemann, P., Noble, A. G., Mets, M., Holfels, E., Withers, S., Latkany, P., and Meier, P. (2006) Outcome of treatment for congenital toxoplasmosis, 1981−2004: The National Collaborative Chicago-Based, Congenital Toxoplasmosis Study. *Clin. Infect. Dis.* 42, 1383−1394.

(3) Boyer, K., Marcinak, J., and McLeod, R. (2009) *Toxoplasma gondii (Toxoplasmosis)*, 3rd ed., Churchill Livingstone, New York.

(4) Hill, D., Coss, C., Dubey, J. P., Wroblewski, K., Sautter, M., Hosten, T., Munoz-Zanzi, C., Mui, E., Withers, S., Boyer, K., Hermes, G., Coyne, J., Jagdis, F., Burnett, A., McLeod, P., Morton, H., Robinson, D., and McLeod, R. (2011) Identification of a sporozoite-specific antigen from *Toxoplasma gondii*. *J. Parasitol.* 97, 328−337.

(5) Boyer, K., Hill, D., Mui, E., Wroblewski, K., Karrison, T., Dubey, J. P., Sautter, M., Noble, A. G., Withers, S., Swisher, C., Heydemann, P., Hosten, T., Babiarz, J., Lee, D., Meier, P., and McLeod, R. (2011) Unrecognized ingestion of *Toxoplasma gondii* oocysts leads to congenital toxoplasmosis and causes epidemics in North America. *Clin. Infect. Dis.* 53, 1081−1089.

(6) Desmonts, G., and Couvreur, J. (1974) Congenital toxoplasmosis. A prospective study of 378 pregnancies. *N. Engl. J. Med.* 290, 1110−1116.

(7) Dubey, J. P., Lindsay, D. S., and Speer, C. A. (1998) Structures of *Toxoplasma gondii* tachyzoites, bradyzoites, and sporozoites and biology and development of tissue cysts. *Clin. Microbiol. Rev.* 11, 267−299.

(8) Dubey, J. P. (2008) The history of *Toxoplasma gondii*: The first 100 years. *J. Eukaryotic Microbiol.* 55, 467−475.

(9) Remington, J. S., McLeod, R., Thulliez, P., and Desmonts, G. (2011) *Toxoplasmosis*, 7th ed., Elsevier Saunders, Philadelphia.

(10) Montoya, J. G., and Liesenfeld, O. (2004) Toxoplasmosis. *Lancet* 363, 1965−1976.

(11) Luft, B. J., and Remington, J. S. (1992) Toxoplasmic encephalitis in AIDS. *Clin. Infect. Dis.* 15, 211−222.

(12) Porter, S. B., and Sande, M. A. (1992) Toxoplasmosis of the central nervous system in the acquired immunodeficiency syndrome. *N. Engl. J. Med.* 327, 1643−1648.

(13) Swisher, C. N., Boyer, K., and McLeod, R. (1994) Congenital toxoplasmosis. The Toxoplasmosis Study Group. *Seminars in Pediatric Neurology 1*, 4−25.

(14) Olariu, T. R., Remington, J. S., McLeod, R., Alam, A., and Montoya, J. G. (2011) Severe congenital toxoplasmosis in the United States: Clinical and serologic findings in untreated infants. *Pediatric Infectious Disease Journal 30*, 1056−1061.

(15) McLeod, R., Mack, D. G., Boyer, K., Mets, M., Roizen, N., Swisher, C., Patel, D., Beckmann, E., Vitullo, D., Johnson, D., et al. (1990) Phenotypes and functions of lymphocytes in congenital toxoplasmosis. *J. Lab. Clin. Med.* 116, 623−635.

(16) McGee, T., Wolters, C., Stein, L., Kraus, N., Johnson, D., Boyer, K., Mets, M., Roizen, N., Beckman, J., Meier, P., et al. (1992) Absence of sensorineural hearing loss in treated infants and children with congenital toxoplasmosis. *Otolaryngol.—Head Neck Surg.* 106, 75−80.

(17) McAuley, J., Boyer, K. M., Patel, D., Mets, M., Swisher, C., Roizen, N., Wolters, C., Stein, L., Stein, M., Schey, W., et al. (1994) Early and longitudinal evaluations of treated infants and children and untreated historical patients with congenital toxoplasmosis: The Chicago Collaborative Treatment Trial. *Clin. Infect. Dis.* 18, 38−72.

(18) McLeod, R., Khan, A. R., Noble, G. A., Latkany, P., Jalbrzikowski, J., and Boyer, K. (2006) Severe sulfadiazine hypersensitivity in a child with reactivated congenital toxoplasmic chorioretinitis. *Pediatric Infectious Disease Journal 25*, 270−272.

(19) Roberts, C. W., McLeod, R., Rice, D. W., Ginger, M., Chance, M. L., and Goad, L. J. (2003) Fatty acid and sterol metabolism: Potential antimicrobial targets in apicomplexan and trypanosomatid parasitic protozoa. *Mol. Biochem. Parasitol.* 126, 129−142.

(20) McFadden, G. I., Reith, M. E., Munholland, J., and Lang-Unnasch, N. (1996) Plastid in human parasites. *Nature 381*, 482.

(21) Kohler, S., Delwiche, C. F., Denny, P. W., Tilney, L. G., Webster, P., Wilson, R. J., Palmer, J. D., and Roos, D. S. (1997) A plastid of probable green algal origin in apicomplexan parasites. *Science 275*, 1485−1489.

(22) Zuther, E., Johnson, J. J., Haselkorn, R., McLeod, R., and Gornicki, P. (1999) Growth of *Toxoplasma gondii* is inhibited by aryloxyphenoxypropionate herbicides targeting acetyl-CoA carboxylase. *Proc. Natl. Acad. Sci. U.S.A. 96*, 13387−13392.

(23) McLeod, R., Muench, S. P., Rafferty, J. B., Kyle, D. E., Mui, E. J., Kirisits, M. J., Mack, D. G., Roberts, C. W., Samuel, B. U., Lyons, R. E., Dorris, M., Milhous, W. K., and Rice, D. W. (2001) Triclosan inhibits the growth of *Plasmodium falciparum* and *Toxoplasma gondii* by inhibition of apicomplexan Fab I. *Int. J. Parasitol. 31*, 109−113.

(24) Ben Mamoun, C., Prigge, S. T., and Vial, H. (2010) Targeting the Lipid Metabolic Pathways for the Treatment of Malaria. *Drug Dev. Res. 71*, 44−55.

(25) Lu, J. Z., Muench, S. P., Allary, M., Campbell, S., Roberts, C. W., Mui, E., McLeod, R. L., Rice, D. W., and Prigge, S. T. (2007) Type I and type II fatty acid biosynthesis in *Eimeria tenella*: Enoyl reductase activity and structure. *Parasitology 134*, 1949−1962.

(26) Mazumdar, J., Wilson, E. H., Masek, K., Hunter, C. A., and Striepen, B. (2006) Apicoplast fatty acid synthesis is essential for organelle biogenesis and parasite survival in *Toxoplasma gondii*. *Proc. Natl. Acad. Sci. U.S.A. 103*, 13192−13197.

(27) Yu, M., Kumar, T. R., Nkrumah, L. J., Coppi, A., Retzlaff, S., Li, C. D., Kelly, B. J., Moura, P. A., Lakshmanan, V., Freundlich, J. S., Valderramos, J. C., Vilcheze, C., Siedner, M., Tsai, J. H., Falkard, B., Sidhu, A. B., Purcell, L. A., Gratraud, P., Kremer, L., Waters, A. P., Schiehser, G., Jacobus, D. P., Janse, C. J., Ager, A., Jacobs, W. R., Jr., Sacchettini, J. C., Heussler, V., Sinnis, P., and Fidock, D. A. (2008) The fatty acid biosynthesis enzyme FabI plays a key role in the development of liver-stage malarial parasites. *Cell Host Microbe 4*, 567−578.

(28) Vaughan, A. M., O'Neill, M. T., Tarun, A. S., Camargo, N., Phuong, T. M., Aly, A. S., Cowman, A. F., and Kappe, S. H. (2009) Type II fatty acid synthesis is essential only for malaria parasite late liver stage development. *Cell. Microbiol. 11*, 506−520.

(29) Falkard, B., Kumar, T. R., Hecht, L. S., Matthews, K. A., Henrich, P. P., Gulati, S., Lewis, R. E., Manary, M. J., Winzeler, E. A., Sinnis, P., Prigge, S. T., Heussler, V., Deschermeier, C., and Fidock, D. (2013) A key role for lipoic acid synthesis during *Plasmodium* liver stage development. *Cell. Microbiol. 15*, 1585−1604.

(30) Magnuson, K., Jackowski, S., Rock, C. O., and Cronan, J. E., Jr. (1993) Regulation of fatty acid biosynthesis in *Escherichia coli. Microbiol. Rev. 57*, 522−542.

(31) Massengo-Tiasse, R. P., and Cronan, J. E. (2009) Diversity in enoyl-acyl carrier protein reductases. *Cell. Mol. Life Sci. 66*, 1507−1517.

(32) Ward, W. H., Holdgate, G. A., Rowsell, S., McLean, E. G., Pauptit, R. A., Clayton, E., Nichols, W. W., Colls, J. G., Minshull, C. A., Jude, D. A., Mistry, A., Timms, D., Camble, R., Hales, N. J., Britton, C. J., and Taylor, I. W. (1999) Kinetic and structural characteristics of the inhibition of enoyl (acyl carrier protein) reductase by triclosan. *Biochemistry 38*, 12514−12525.

(33) Rozwarski, D. A., Grant, G. A., Barton, D. H., Jacobs, W. R., Jr., and Sacchettini, J. C. (1998) Modification of the NADH of the isoniazid target (InhA) from *Mycobacterium tuberculosis. Science 279*, 98−102.

(34) Grassberger, M. A., Turnowsky, F., and Hildebrandt, J. (1984) Preparation and antibacterial activities of new 1,2,3-diazaborine derivatives and analogues. *J. Med. Chem. 27*, 947−953.

(35) Tipparaju, S. K., Muench, S. P., Mui, E. J., Ruzheinikov, S. N., Lu, J. Z., Hutson, S. L., Kirisits, M. J., Prigge, S. T., Roberts, C. W., Henriquez, F. L., Kozikowski, A. P., Rice, D. W., and McLeod, R. L. (2010) Identification and development of novel inhibitors of *Toxoplasma gondii* enoyl reductase. *J. Med. Chem. 53*, 6287−6300.

(36) Cherednichenko, G., Zhang, R., Bannister, R. A., Timofeyev, V., Li, N., Fritsch, E. B., Feng, W., Barrientos, G. C., Schebb, N. H., Hammock, B. D., Beam, K. G., Chiamvimonvat, N., and Pessah, I. N. (2012) Triclosan impairs excitation-contraction coupling and Ca^{2+} dynamics in striated muscle. *Proc. Natl. Acad. Sci. U.S.A. 109*, 14158−14163.

(37) Cheng, G., Muench, S. P., Zhou, Y., Afanador, G. A., Mui, E. J., Fomovska, A., Lai, B. S., Prigge, S. T., Woods, S., Roberts, C. W., Hickman, M. R., Lee, P. J., Leed, S. E., Auschwitz, J. M., Rice, D. W., and McLeod, R. (2013) Design, synthesis, and biological activity of diaryl ether inhibitors of *Toxoplasma gondii* enoyl reductase. *Bioorg. Med. Chem. Lett. 23*, 2035−2043.

(38) Stec, J., Fomovska, A., Afanador, G. A., Muench, S., Zhou, Y., Lai, B. S., El Bissati, K., Hickman, M. R., Lee, P. J., Leed, S. E., Auschwitz, J. M., Sommerville, C., Woods, S., Roberts, C., Rice, D., Prigge, S. T., McLeod, R., and Kozikowski, A. P. (2013) Modification of Triclosan Scaffold in Search of Improved Inhibitors for Enoyl-Acyl Carrier Protein (ACP) Reductase in *Toxoplasma gondii. ChemMedChem 8*, 1138−1160.

(39) Samuel, B. U., Hearn, B., Mack, D., Wender, P., Rothbard, J., Kirisits, M. J., Mui, E., Wernimont, S., Roberts, C. W., Muench, S. P., Rice, D. W., Prigge, S. T., Law, A. B., and McLeod, R. (2003) Delivery of antimicrobials into parasites. *Proc. Natl. Acad. Sci. U.S.A. 100*, 14281−14286.

(40) Freundlich, J. S., Anderson, J. W., Sarantakis, D., Shieh, H. M., Yu, M., Valderramos, J. C., Lucumi, E., Kuo, M., Jacobs, W. R., Jr., Fidock, D. A., Schiehser, G. A., Jacobus, D. P., and Sacchettini, J. C. (2005) Synthesis, biological activity, and X-ray crystal structural analysis of diaryl ether inhibitors of malarial enoyl acyl carrier protein reductase. Part 1: 4′-Substituted triclosan derivatives. *Bioorg. Med. Chem. Lett. 15*, 5247−5252.

(41) Freundlich, J. S., Wang, F., Tsai, H. C., Kuo, M., Shieh, H. M., Anderson, J. W., Nkrumah, L. J., Valderramos, J. C., Yu, M., Kumar, T. R. S., Valderramos, S. G., Jacobs, W. R., Schiehser, G. A., Jacobus, D. P., Fidock, D. A., and Sacchettini, J. C. (2007) X-ray structural analysis of plasmodium falciparum enoyl acyl carrier protein reductase as a pathway toward the optimization of triclosan antimalarial efficacy. *J. Biol. Chem. 282*, 25436−25444.

(42) Freundlich, J. S., Wang, F., Vilcheze, C., Gulten, G., Langley, R., Schiehser, G. A., Jacobus, D. P., Jacobs, W. R., Jr., and Sacchettini, J. C. (2009) Triclosan derivatives: Towards potent inhibitors of drug-sensitive and drug-resistant *Mycobacterium tuberculosis. ChemMedChem 4*, 241−248.

(43) Freundlich, J. S., Yu, M., Lucumi, E., Kuo, M., Tsai, H. C., Valderramos, J. C., Karagyozov, L., Jacobs, W. R., Jr., Schiehser, G. A., Fidock, D. A., Jacobus, D. P., and Sacchettini, J. C. (2006) Synthesis and biological activity of diaryl ether inhibitors of malarial enoyl acyl carrier protein reductase. Part 2: 2′-Substituted triclosan derivatives. *Bioorg. Med. Chem. Lett. 16*, 2163−2169.

(44) Lo, M. C., Aulabaugh, A., Jin, G., Cowling, R., Bard, J., Malamas, M., and Ellestad, G. (2004) Evaluation of fluorescence-based thermal shift assays for hit identification in drug discovery. *Anal. Biochem. 332*, 153−159.

(45) Matulis, D., Kranz, J. K., Salemme, F. R., and Todd, M. J. (2005) Thermodynamic stability of carbonic anhydrase: Measurements of binding affinity and stoichiometry using ThermoFluor. *Biochemistry 44*, 5258−5266.

(46) Niesen, F. H., Berglund, H., and Vedadi, M. (2007) The use of differential scanning fluorimetry to detect ligand interactions that promote protein stability. *Nat. Protoc. 2*, 2212−2221.

(47) Muench, S. P., Prigge, S. T., Zhu, L., Kirisits, M. J., Roberts, C. W., Wernimont, S., McLeod, R., and Rice, D. W. (2006) Expression, purification and preliminary crystallographic analysis of the *Toxoplasma gondii* enoyl reductase. *Acta Crystallogr. F62*, 604−606.

(48) Pantoliano, M. W., Petrella, E. C., Kwasnoski, J. D., Lobanov, V. S., Myslik, J., Graf, E., Carver, T., Asel, E., Springer, B. A., Lane, P., and Salemme, F. R. (2001) High-density miniaturized thermal shift assays as a general strategy for drug discovery. *J. Biomol. Screening 6*, 429−440.

(49) Goodsell, D. S., Morris, G. M., and Olson, A. J. (1996) Automated docking of flexible ligands: Applications of AutoDock. *J. Mol. Recognit. 9*, 1−5.

(50) Guex, N., and Peitsch, M. C. (1997) SWISS-MODEL and the Swiss-PdbViewer: An environment for comparative protein modeling. *Electrophoresis 18*, 2714−2723.

(51) Muench, S. P., Prigge, S. T., McLeod, R., Rafferty, J. B., Kirisits, M. J., Roberts, C. W., Mui, E. J., and Rice, D. W. (2007) Studies of

Toxoplasma gondii and *Plasmodium falciparum* enoyl acyl carrier protein reductase and implications for the development of antiparasitic agents. *Acta Crystallogr. D63*, 328−338.

(52) Miller, W. H., Seefeld, M. A., Newlander, K. A., Uzinskas, I. N., Burgess, W. J., Heerding, D. A., Yuan, C. C., Head, M. S., Payne, D. J., Rittenhouse, S. F., Moore, T. D., Pearson, S. C., Berry, V., DeWolf, W. E., Jr., Keller, P. M., Polizzi, B. J., Qiu, X., Janson, C. A., and Huffman, W. F. (2002) Discovery of aminopyridine-based inhibitors of bacterial enoyl-ACP reductase (FabI). *J. Med. Chem. 45*, 3246−3256.

(53) Todd, M. J. (2005) Affinity assays for decrypting protein targets of unknown function. *Drug Discovery Today: Technol. 2*, 267−273.

(54) Cummings, M. D., Farnum, M. A., and Nelen, M. I. (2006) Universal screening methods and applications of ThermoFluor. *J. Biomol. Screening 11*, 854−863.

(55) Lea, W. A., and Simeonov, A. (2012) Differential scanning fluorometry signatures as indicators of enzyme inhibitor mode of action: Case study of glutathione S-transferase. *PLoS One 7*, e36219.

(56) Vedadi, M., Niesen, F. H., Allali-Hassani, A., Fedorov, O. Y., Finerty, P. J., Jr., Wasney, G. A., Yeung, R., Arrowsmith, C., Ball, L. J., Berglund, H., Hui, R., Marsden, B. D., Nordlund, P., Sundstrom, M., Weigelt, J., and Edwards, A. M. (2006) Chemical screening methods to identify ligands that promote protein stability, protein crystallization, and structure determination. *Proc. Natl. Acad. Sci. U.S.A. 103*, 15835−15840.

(57) Ericsson, U. B., Hallberg, B. M., Detitta, G. T., Dekker, N., and Nordlund, P. (2006) Thermofluor-based high-throughput stability optimization of proteins for structural studies. *Anal. Biochem. 357*, 289−298.

(58) Kapoor, M., Mukhi, P. L., Surolia, N., Suguna, K., and Surolia, A. (2004) Kinetic and structural analysis of the increased affinity of enoyl-ACP (acyl-carrier protein) reductase for triclosan in the presence of NAD^+. *Biochem. J. 381*, 725−733.

(59) Perozzo, R., Kuo, M., Sidhu, A., Valiyaveettil, J. T., Bittman, R., Jacobs, W. R., Jr., Fidock, D. A., and Sacchettini, J. C. (2002) Structural elucidation of the specificity of the antibacterial agent triclosan for malarial enoyl acyl carrier protein reductase. *J. Biol. Chem. 277*, 13106−13114.

(60) Kapoor, M., Dar, M. J., Surolia, A., and Surolia, N. (2001) Kinetic determinants of the interaction of enoyl-ACP reductase from *Plasmodium falciparum* with its substrates and inhibitors. *Biochem. Biophys. Res. Commun. 289*, 832−837.

(61) Sivaraman, S., Sullivan, T. J., Johnson, F., Novichenok, P., Cui, G., Simmerling, C., and Tonge, P. J. (2004) Inhibition of the bacterial enoyl reductase FabI by triclosan: A structure-reactivity analysis of FabI inhibition by triclosan analogues. *J. Med. Chem. 47*, 509−518.

(62) Marcinkeviciene, J., Jiang, W., Kopcho, L. M., Locke, G., Luo, Y., and Copeland, R. A. (2001) Enoyl-ACP reductase (FabI) of *Haemophilus influenzae*: Steady-state kinetic mechanism and inhibition by triclosan and hexachlorophene. *Arch. Biochem. Biophys. 390*, 101−108.

(63) Lee, J. H., Park, A. K., Chi, Y. M., Moon, J. H., and Lee, K. S. (2011) Crystallization and preliminary X-ray crystallographic studies of enoyl-acyl carrier protein reductase (FabI) from *Psuedomonas aeruginosa*. *Acta Crystallogr. F67*, 214−216.

(64) Kapoor, M., Reddy, C. C., Krishnasastry, M. V., Surolia, N., and Surolia, A. (2004) Slow-tight-binding inhibition of enoyl-acyl carrier protein reductase from *Plasmodium falciparum* by triclosan. *Biochem. J. 381*, 719−724.

(65) Yamada, K., Hara, N., Shibata, T., Osago, H., and Tsuchiya, M. (2006) The simultaneous measurement of nicotinamide adenine dinucleotide and related compounds by liquid chromatography/electrospray ionization tandem mass spectrometry. *Anal. Biochem. 352*, 282−285.

(66) Houtkooper, R. H., Canto, C., Wanders, R. J., and Auwerx, J. (2010) The secret life of NAD^+: An old metabolite controlling new metabolic signaling pathways. *Endocr. Rev. 31*, 194−223.

(67) Yang, H., Yang, T., Baur, J. A., Perez, E., Matsui, T., Carmona, J. J., Lamming, D. W., Souza-Pinto, N. C., Bohr, V. A., Rosenzweig, A., de Cabo, R., Sauve, A. A., and Sinclair, D. A. (2007) Nutrient-sensitive mitochondrial NAD^+ levels dictate cell survival. *Cell 130*, 1095−1107.

(68) Wilhelm, F., and Hirrlinger, J. (2011) The NAD^+/NADH redox state in astrocytes: Independent control of the NAD^+ and NADH content. *J. Neurosci. Res. 89*, 1956−1964.

(69) Hara, N., Yamada, K., Shibata, T., Osago, H., Hashimoto, T., and Tsuchiya, M. (2007) Elevation of cellular NAD levels by nicotinic acid and involvement of nicotinic acid phosphoribosyltransferase in human cells. *J. Biol. Chem. 282*, 24574−24582.